Supplementary Information

Conformational dynamics of influenza A virus ribonucleoprotein complexes during RNA synthesis.

Diego Carlero[1]¶, Shingo Fukuda[2]¶, Rebeca Bocanegra[3,4]¶, Toshio Ando[2], Jaime Martin-Benito[1]*, Borja Ibarra[3,4]**

[1]Centro Nacional de Biotecnología, Campus de Cantoblanco, Madrid, Spain.

[2]WPI Nano Life Science Institute (WPI-NanoLSI), Kanazawa University, Kakuma-machi, Kanazawa 920-1192, Japan.

[3]Instituto Madrileño de Estudios Avanzados en Nanociencia, IMDEA Nanociencia, Madrid, Spain.

[4]IMDEA Nanociencia & CNB-CSIC-IMDEA Nanociencia Associated Unit "Unidad de Nanobiotecnología", Madrid, Spain.

¶These authors contributed equally to this work

*Corresponding authors

*Corresponding authors: shingofukuda@staff.kanazawa-u.ac.jp; jmartinb@cnb.csic.es; borja.ibarra@imdea.org

SUPPLEMENTARY METHODS

Production, purification and functional characterization of rRNPs

rRNPs carrying a 352-nt fragment of influenza A virus (IAV) NS genomic vRNA were produced and amplified in vivo by introducing plasmids pGPB1, pGPB2His, pGPA, pGNP(polyA), and pT7ΔNSRT clone 49 into COS1 cells infected with vaccinia vTF7-3. Clarified cell extracts were subjected to overnight incubation at 4 °C with Ni-NTA-agarose resin in 50 mM Tris-HCl (pH 8.0), 100 mM KCl, 5 mM $MgCl_2$, 0.5% IGEPAL, 20 mM imidazole, 1 U/µl RNAsin, and an EDTA-free protease inhibitor cocktail. Subsequently, the resin was washed with 100 volumes of 50 mM Tris-HCl (pH 8), 100 mM KCl, 5 mM $MgCl_2$, 0.5% IGEPAL, and 20-50 mM imidazole. rRNPs were eluted in 50 mM Tris-HCl (pH 8.0), 100 mM KCl, 5 mM $MgCl_2$, 0.5% IGEPAL, and 150 mM imidazole.

HS-AFM tip preparation and image acquisition

An electron beam deposition (EBD) tip was grown for 1.5 minutes on the original tip of the cantilever in an atmosphere of sublimated ferrocene vapor using a field emission scanning electron microscope (SUPRA40VP, Zeiss, Germany). The grown EBD tip was sharpened by radiofrequency plasma etching for 1 min at 15 W in an argon environment using a plasma cleaner (Tergeo Plasma Cleaner, PIE Scientific, USA). For HS-AFM image acquisition, we used a scan range of 6 × 6 µm^2 lateral and 1 µm vertical. Initially, we set the wide-area scanner to a range between 500 × 500 and 1000 × 1000 nm^2 to find active molecules. Then we moved the stage to place the molecule at the cantilever position and observed it with a scan range between 100 × 100 and 200 × 200 nm^2 at 1-2 frames/ s for 120 s. Individual frames from HS-AFM movies were processed using customized algorithms written in IGOR Pro (WaveMetrics, USA). First, spike noise in each image was reduced by Gaussian filtering, followed by a flattening filter to remove the substrate-tilt effect. Second, a target molecule was tracked using a two-dimensional correlation method to eliminate effects of lateral diffusion of the molecule and the mechanical drift[1] . Briefly, a region of interest (ROI) in a first frame is chosen as reference for aligning subsequent frames using 2D cross correlation.

$$CCV = \frac{\sum_m \sum_n (H_{m,n} - \overline{H})(I_{m,n} - \overline{I})}{\sqrt{(\sum_m \sum_n (H_{m,n} - \overline{H})^2)} \sqrt{(\sum_m \sum_n (I_{m,n} - \overline{I})^2)}} \qquad (1)$$

where H and I denote the height values at a pixel point (m,n) for the targeted ROI at different time points and the initial one (from the first frame), respectively. $\overline{H}$ and $\overline{I}$ are height mean values of the matrix. The region of the maximal correlation coefficient of variation (CCV) value that was found defines the corrected origin of the image.

Electron microscopy imaging and analysis

For the analysis of RNA synthesis with negative staining electron microscopy, rRNPs were incubated in the reaction buffer containing 1 U/µl RNasin, 100 µM ApG, 1 mM NTPs and 12.5 µM of the non-hydrolysable nucleotide analogue UpNHpp (ratio UTP:UpNHpp 80:1) at 30 °C for 3 h. After incubation, 5 µl aliquots of the rRNP sample were applied to glow-discharged, carbon-coated grids for 5 min. Subsequently, the samples were subjected to three washes and stained for 1 min with a 2% (w/v) solution of uranyl acetate. The grids were then transferred to a JEOL 1400 Flash electron microscope equipped with a side-entry holder and operated at 120 kV. Images were captured using SerialEM software on a Gatan One View camera at 80.7K magnification, following low-dose protocols with a sampling ratio of 2.26 Å per pixel and defocus ranging from 1.5 to 3.5 µm.

For image processing, operations were carried out using the Xmipp[2,3] and RELION[4] processing packages within the Scipion platform (http://scipion.i2pc.es/[5]). The degree of defocusing of each micrograph was calculated by analyzing its Fourier transform using the Ctffind4 program[6]. Particles were selected using Xmipp particle picker to obtain the final indicated number of items, which were extracted and normalized using Xmipp. Once extracted with a size of 200x200 pixels (2.26 Å/ pixel) the particles were subjected to an unsupervised 2D classification using RELION to separate the images into the different classes representing the different states acquired by the complex during the RNA production process.

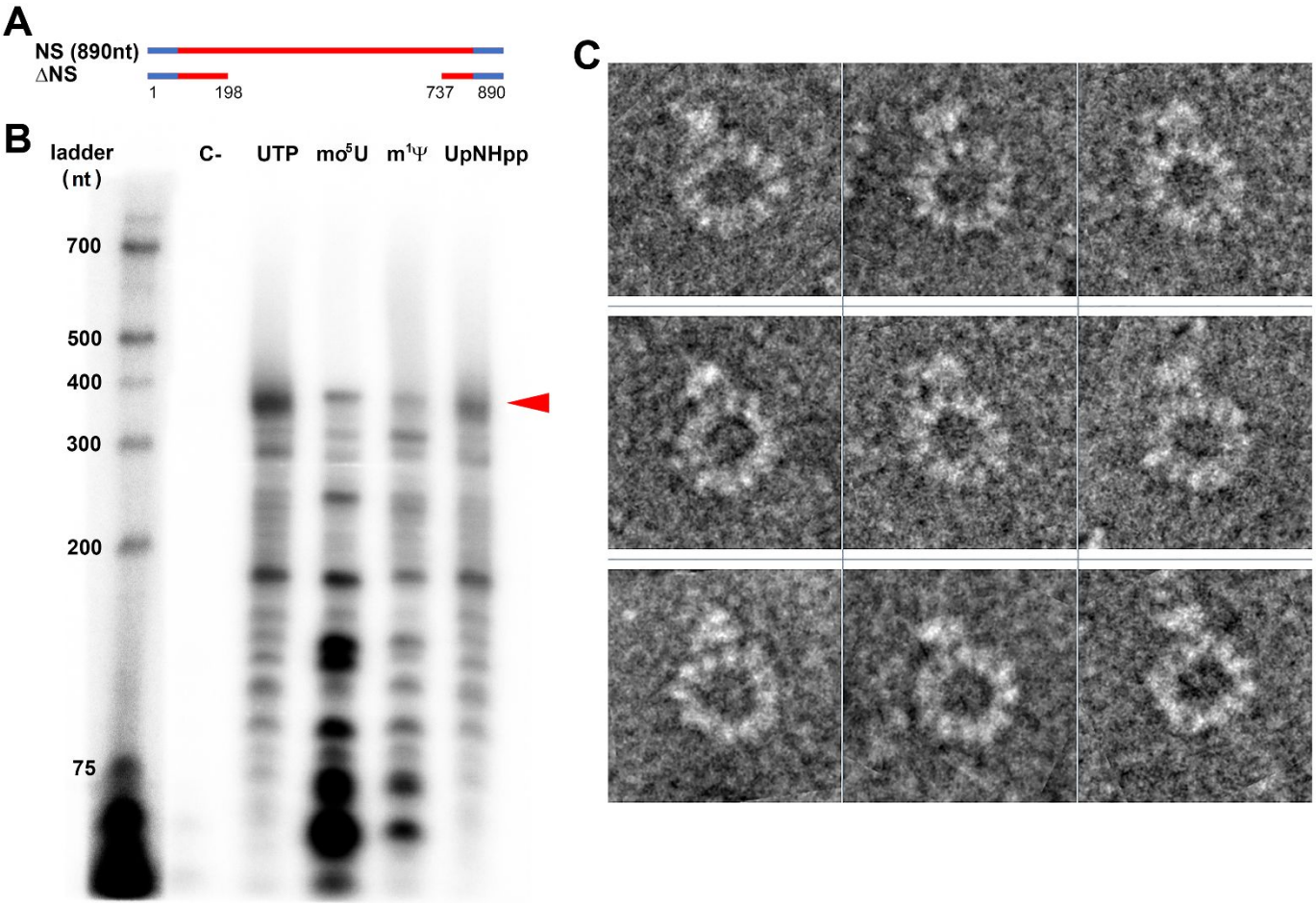

Supplementary Figure 1. Template length and *in vitro* transcription activity of rRNPs. A) Diagram of the influenza A virus (IAV) Non-Structural protein 1 ssRNA segment 8 (NS) and its truncated derivative (ΔNS), which lacks 539 nt (from 198 to 737) from the internal coding region. ΔNS presents a total length of 352 nt and was used in this work to reconstitute the annular recombinant RNPs (rRNPs)[7]. Blue regions at both ends represent the conserved sequences among all influenza virus RNA segments[8]. **B)** rRNPs are active in the presence of uracil derivatives. Acrylamide gel electrophoresis analysis of RNA synthesis activity of rRNPs *in vitro*. rRNPs were incubated for 1 h at 30 °C in the reaction buffer (50 mM Tris-HCl, pH 8.0, 2 mM $MgCl_2$, 100 mM KCl, and 1 mM DTT) supplemented with 100 µM ApG, 1 µM GTP, 10 µCi of αP32-GTP (3,000 Ci/mmol), 1 mM ATP, 1 mM CTP and (from left to right) either 1 mM UTP, 1 mM 5-methoxy-uridine (mo^5U), 1 mM methyl-pseudouridine ($m^1\Psi$), or UTP:UpNHpp (80:1). "C-" is a control condition with the absence of UTP in the reaction buffer. Red arrow shows the position of the full-length nascent ssRNA (~350 nt). It is noteworthy that the production of RNA in the presence of mo^5U is significantly greater compared to that with the other two analogs or with natural UTP. This result is in agreement with HS-AFM results showing that incorporation of mo^5U increase the RNA synthesis reaction (Figure 3B). Additionally, incorporation of mo^5U increases the amount of RNA fragments shorter than ~100 nucleotides. This may be the result of an increased number of abortive RNA synthesis cycles under these conditions. The conformational changes of rRNPs undergoing abortive RNA synthesis would last less than 1-2 seconds, according to the average velocity of RNA synthesis at 1 mM NTP/mo5U (~ 50 nt/s, Figure 3B). Consequently, these rapid events would likely remain undetected under HS-AFM observation conditions. Further investigation is required to determine whether the premature interruption of RNA synthesis correlates with the stability of the secondary structure of the nascent RNA. C) Gallery of representative EM images of rRNPs complexes in the absence of NTPs/ApG.

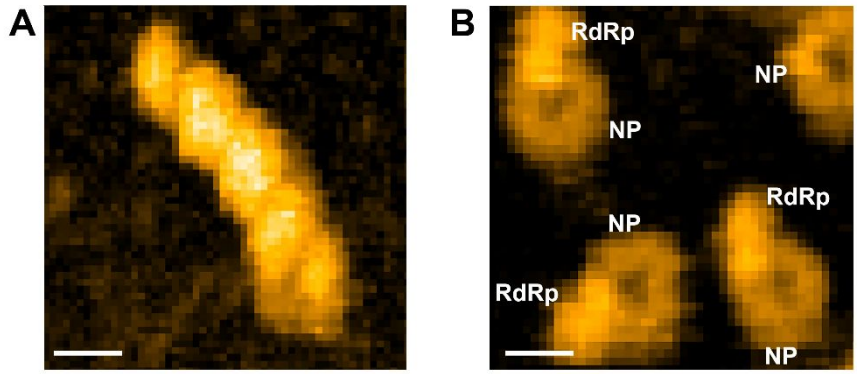

Supplementary Figure 2. HS-AFM imaging of native and recombinant RNPs.
A) HS-AFM video frame of a native IAV vRNP deposited on bare mica, showing the characteristic helical conformation of these RNP complexes. In these images the position of the RdRp cannot be distinguished from the NP-RNA template. **B)** HS-AFM field of annular rRNPs. The short length of the RNA template (352 nt) prevents the NP-RNA template from adopting a helical conformation and favors an annular shape where the RdRp and the NP-RNA template are clearly distinguishable; scale bars in both figures = 20 nm.

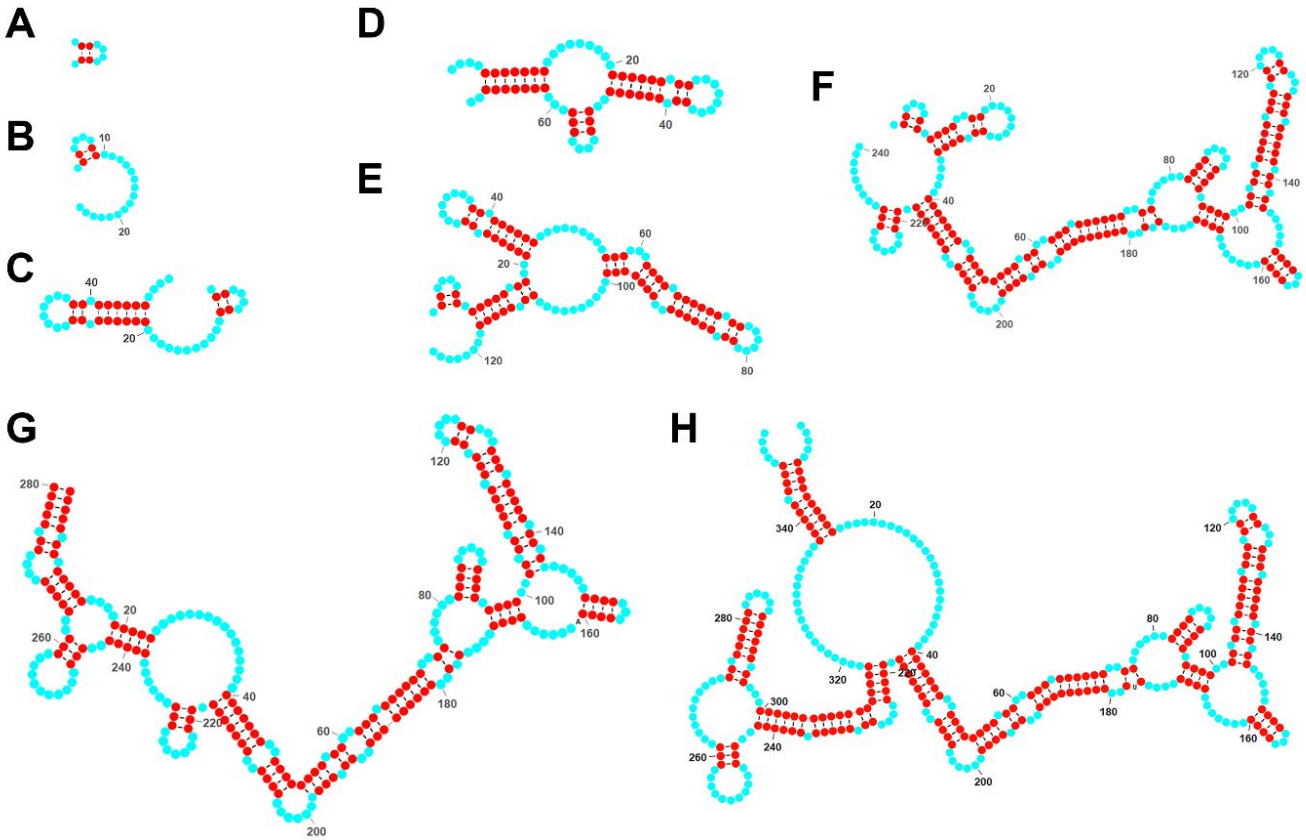

Supplementary Figure 3. Predicted secondary structures of nascent RNA at different stages of RNA synthesis. UNAfold predictions of the most stable secondary structures of different lengths of the nascent RNA (37 ºC and 1 M NaCl). (A) 10 nt, (B) 25 nt, (C) 50 nt, (D) 75 nt, (E) 125 nt, (F) 240 nt, (G) 280 nt and (H) 352 nt (full-length molecule)[9]. Annealed bases are depicted in red and free bases in cyan; RNA representation was done in RNA canvas [10].

Supplementary Table 1. Number of active, independent rRNPs measured using HS-AFM in reaction mixtures containing different concentrations of the four natural NTPs (UTP) or N^1-methyl-pseudouridine ($m^1\Psi$) or 5-methoxy-uridine (mo^5U) instead of UTP.

	25 μM	50 μM	100 μM	400 μM	1000 μM
UTP	6	6	10	10	7
mo^5U	9	6	13	9	7
$m^1\Psi$	--	15	16	11	9

Supplementary video 1. rRNP organization is stable under HS-AFM experimental conditions. HSAFM video of a single rRNP in the reaction buffer without NTPs. The rRNP preserves the structural organization and height profile under scanning times longer than 100 s. Imaging rate 2 fps, scale bar =20nm. For more information, see main text and Figure 1.

Supplementary video 2. Mosaic of 3 additional HS-AFM videos of independent rRNPs in the reaction buffer without NTPs. Imaging rate 2 fps, scale bar =20nm.

Supplementary video 3. Conformational changes of a single rRNP in the presence of ApG/NTPs. HS-AFM video of a single rRNP in the reaction buffer containing NTPs (100 μM) and ApG primer (100 μM). Under RNA competent conditions, the rRNP loses its annular organization and goes through conformational transitions before returning to its initial conformation. Imaging rate 1 fps (scale bar =20nm). For more information, see main text and Figure 1.

Supplementary video 4. The conformational change of the rRNPs is halted in the presence of UpNHpp. HS-AFM video of a single rRNP in the reaction buffer containing ApG (100 μM) and an NTP mixture (100 μM) including the non-hydrolysable UTP analog UpNHpp (2 μM). Interference of RNA synthesis by UpNHpp prevents the rRNP from recovering its initial annular organization. Imaging rate 2 fps (scale bar = 20 nm). For more information, see main text and Figure 2.

Supplementary video 5. Conformational cycle at 25 μM NTP concentration. HS-AFM video of a single rRNP in the reaction buffer containing NTPs (25 μM) and ApG primer (100 μM). Imaging rate 1fps (scale bar =20nm). For more information, see main text and Figure 3.

Supplementary video 6. Conformational cycle at 50 μM NTP concentration. HS-AFM video of a single rRNP in the reaction buffer containing NTPs (50 μM) and ApG primer (100 μM). Imaging rate 1fps (scale bar =20nm). For more information, see main text and Figure 3.

Supplementary video 7. Conformational cycle at 400 μM NTP concentration. HS-AFM video of a single rRNP in the reaction buffer containing NTPs (400 μM) and ApG primer (100 μM). Imaging rate 1fps (scale bar =20nm). For more information, see main text and Figure 3.

Supplementary video 8. Mosaic of 6 additional HS-AFM videos of independent rRNPs in the reaction buffer containing NTPs. Videos are arranged from higher (top left) to lower (bottom right) NTPs concentrations. Imaging rate 1 fps, scale bar =20nm.

Supplementary video 9. Mosaic of 6 HS-AFM videos of independent rRNPs in the reaction buffer containing mo^5U/ NTP. Videos are arranged from higher (top left) to lower (bottom right) mo^5U/ NTPs concentrations. Imaging rate 1 fps, scale bar =20nm.

Supplementary video 10. Mosaic of 6 HS-AFM videos of independent rRNPs in the reaction buffer containing $m^1\Psi$/ NTP. Videos are arranged from higher (top left) to lower (bottom right) $m^1\Psi$/ NTPs concentrations. Imaging rate 1 fps, scale bar =20nm.

Supplementary video 11. Consecutive conformational cycles of individual rRNPs during RNA synthesis. HS-AFM video of a single rRNP undergoing two consecutive conformational changes in a reaction buffer containing NTPs (50 μM) and ApG primer (100 μM). Each cycle would correspond with the synthesis of a nascent RNA complementary to the entire RNA template. Imaging rate 1fps (scale bar =20nm). For more information, see main text and Figure 4.

Supplementary video 12. Mosaic of 3 additional HS-AFM videos of independent rRNPs undergoing consecutive conformational cycles.

Supplementary animation 1: The animation illustrates the conformational cycle depicted in Figure 1F.

Supplementary references

1. Uchihashi, T., Iino, R., Ando, T. & Noji, H. High-Speed Atomic Force Microscopy Reveals Rotary Catalysis of Rotorless F_1 -ATPase. *Science (1979)* **333**, 755–758 (2011).
2. de la Rosa-Trevín, J. M. *et al.* Xmipp 3.0: An improved software suite for image processing in electron microscopy. *J Struct Biol* **184**, 321–328 (2013).
3. Scheres, S. H. W., Núñez-Ramírez, R., Sorzano, C. O. S., Carazo, J. M. & Marabini, R. Image processing for electron microscopy single-particle analysis using XMIPP. *Nat Protoc* **3**, 977–990 (2008).
4. Scheres, S. H. W. RELION: Implementation of a Bayesian approach to cryo-EM structure determination. *J Struct Biol* **180**, 519–530 (2012).
5. de la Rosa-Trevín, J. M. *et al.* Scipion: A software framework toward integration, reproducibility and validation in 3D electron microscopy. *J Struct Biol* **195**, 93–99 (2016).
6. Rohou, A. & Grigorieff, N. CTFFIND4: Fast and accurate defocus estimation from electron micrographs. *J Struct Biol* **192**, 216–221 (2015).
7. Ortega, J. *et al.* Ultrastructural and Functional Analyses of Recombinant Influenza Virus Ribonucleoproteins Suggest Dimerization of Nucleoprotein during Virus Amplification. *J Virol* **74**, 156–163 (2000).
8. Hsu, M. T., Parvin, J. D., Gupta, S., Krystal, M. & Palese, P. Genomic RNAs of influenza viruses are held in a circular conformation in virions and in infected cells by a terminal panhandle. *Proceedings of the National Academy of Sciences* **84**, 8140–8144 (1987).
9. Markham, N. R. & Zuker, M. UNAFold. in 3–31 (2008). doi:10.1007/978-1-60327-429-6_1.
10. Johnson, P. Z. & Simon, A. E. RNAcanvas: interactive drawing and exploration of nucleic acid structures. *Nucleic Acids Res* **51**, W501–W508 (2023).